A High-Efficiency and Long-Distance Power-Relay System With Equal Power Distribution

Fei Lu, *Member, IEEE*, Hua Zhang, *Member, IEEE*, Weiguo Li, *Member, IEEE*, Zhe Zhou, Chong Zhu, *Member, IEEE*, Chenwen Cheng, Zhanfeng Deng, Xi Chen, *Senior Member, IEEE*, and Chunting Chris Mi, *Fellow, IEEE*

***Abstract*— This paper proposes a wireless power repeater system for long-distance and multiple-load applications with equal power load at each repeater. Each repeater performs as a power relay that not only receives and transmits power but also supplies power to its local load. The main contribution of this paper is to provide the design methodology of a distributed power-relay system. First, it provides the mathematical model of the power distribution among the power relays, indicating that the inductances and resistances can affect the power distribution. Second, it provides the power transfer capability of a power-relay system based on the quality factor and efficiency requirement, indicating the maximum achievable number of power relays in a system. Aiming at practical applications, this paper provides the guideline for the circuit parameter design to achieve equal power distribution. Two typical examples are proposed to realize equal power distribution. The identical M_n and different R_n examples are selected for implementation. The coil size is 400 mm × 400 mm, and the eight power relays achieve a transfer distance of 3.2 m with a total power of 760 W and an efficiency of 70%. Experimental results validate that equal power distribution is achieved for the multiple loads across a long distance. Each power relay dissipates about 95-W power in its local load with a power variation limited to ±2%.**

***Index Terms*— Equal power distribution, long distance, magnetic field repeater, multiple loads, power relay.**

I. Introduction

INDUCTIVE power transfer (IPT) technology utilizes high-frequency magnetic fields to transfer power and has been widely used in both low- and high-power applications to charge the electronic devices and electric vehicles [1]–[3]. The switching frequency is in the kilohertz to megahertz range, resulting in a near-field IPT system. The effective transfer distance is, therefore, around the physical size of the transmitter [4], [5]. Usually, the system power and efficiency decrease with an increasing transfer distance because the coupling coefficient between the transmitter and receiver coils drops rapidly with distance [6], [7]. For example, a dipole transmitter with a size of 2 m can deliver several Watts power to a load at several meters away with relatively low efficiency [8]. To achieve effective long-distance wireless power transfer, the magnetic field repeater system can be a good solution [9], [10], and it mainly has two advantages.

First, the magnetic field repeater system can transfer power with acceptable efficiency for a long-distance application. In a general IPT system, the magnetic field strength attenuates with an increasing distance, leading to the decreasing of power and efficiency. However, due to the appearance of repeater coils, the magnetic field can be continuously enhanced along the power transfer route [11]–[13]. Therefore, sufficient power transfer can be realized, and the efficiency can be improved [14], [15].

Second, the magnetic field repeater system has the capability to supply power to multiple loads [16], [17] and guide the power transfer direction [18]. Each repeater acts as a power relay that not only has interactive power exchange with the other coils but also provides part of the received power to its local load, resulting in a single-input multiple-output or distributed IPT system [19]–[22]. Therefore, the balancing of power distribution among different power relays is an important design criterion in a multiple-load system. Meanwhile, the power relays can be arranged in different shapes, and their relative position can also vary, which provides the flexibility in designing the system structure [23]–[25].

Compared to the previous literature [11]–[25], the main contribution of this paper is the design methodology of a distributed power-relay IPT system, which can be summarized into two aspects.

First, it investigates the mathematic model of the power distribution among the power relays with regard to the circuit parameters, such as the coil inductances and load resistances. Based on the calculated model, a guideline is provided to design the circuit parameters in order to achieve equal power distribution. Also, two design examples are provided to validate the proposed method, showing that adjusting the

Manuscript received August 9, 2018; revised November 16, 2018; accepted January 21, 2019. Date of publication February 7, 2019; date of current version May 6, 2020. This work was supported by Global Energy Interconnection Research Institute Co. Ltd., through the State Grid Sci and Tech Project "Research on the Magnetic-Resonant Wireless Power Transfer Technology for the High-Voltage Converter Valve in FACTS" under Grant GEIRI-DL-71-17-011. Recommended for publication by Associate Editor Ron Hui. *(Corresponding author: Chunting Chris Mi.)*

F. Lu and H. Zhang are with the Department of Electrical and Computer Engineering, Drexel University, Philadelphia, PA 19104 USA (e-mail: fei.lu@drexel.edu; hua.zhang@drexel.edu).

W. Li, Z. Zhou, and Z. Deng are with the State Key Laboratory of Advanced Power Transmission Technology (Global Energy Interconnection Research Institute), Beijing 102211, China (e-mail: lwgmb90549@sina.com; zhouzhe@geiri.sgcc.com.cn; iphone21@sina.com).

C. Zhu, C. Cheng, and C. C. Mi are with the Department of Electrical and Computer Engineering, San Diego State University, San Diego, CA 92182 USA (e-mail: chong.zhu@sdsu.edu; cheng.cwen@sdsu.edu; cmi@sdsu.edu).

X. Chen is with the Global Energy Interconnection Research Institute North America, San Jose, CA 95134 USA (e-mail: xi.chen@geirina.net).

Color versions of one or more of the figures in this article are available online at http://ieeexplore.ieee.org.

Digital Object Identifier 10.1109/JESTPE.2019.2898125

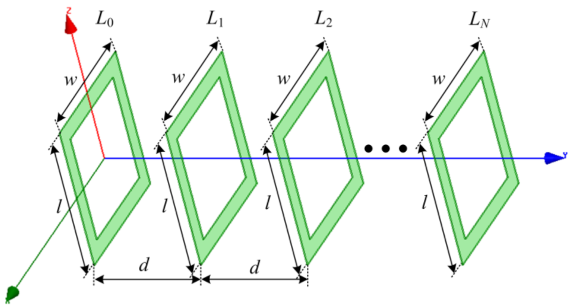

Fig. 1. Structure of a long-distance magnetic field repeater system with a transmitter and N power relays.

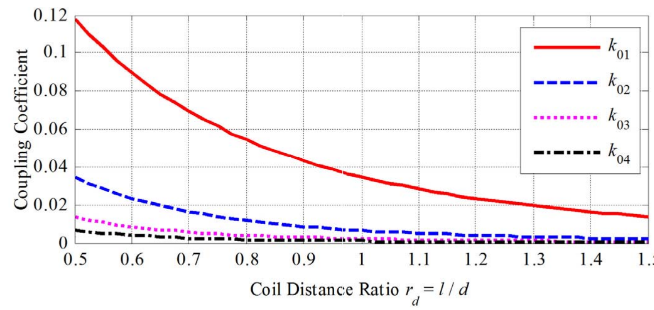

Fig. 2. Maxwell-simulated coupling coefficient between the transmitter and the power-relay coils at different values of distance ratio $r_d = d/l$.

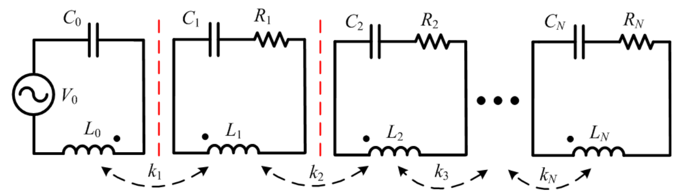

Fig. 3. Circuit topology of a power-relay system with a transmitter and N receivers.

inductances and resistances can both help to achieve equal power distribution.

Second, it studies the power transfer capability of a power-relay system, considering the power loss in the passive components and the efficiency requirement. It can answer a straightforward question—how many power relays we can support in a system given the quality factor and efficiency requirement. In other words, it provides the maximum achievable number of power relays in an IPT system that can realize effective power transfer at different values of the component quality factor. This is very useful and valuable to guide us in designing a power-relay system for the practical applications.

In addition, compared to the previous literature [11]–[25], the other important contribution is that this paper aims at practical applications considering the power distribution property, such as powering a series of electronic devices, which can contribute to realizing a smart building [26], wireless TVs [27], and other appliances [28]. Also, it can be used in the smart grid area [29]. For example, in order to supply power to the gate driver circuits of insulated gate bipolar transistors in a flexible ac transmission system (FACTS), the power-relay solution is a good choice with a reliable high-voltage isolation capability. Since the gate drivers in a FACTS system usually require an equal amount of power for each gate driver, this paper focuses on an equal power distributed system to multiple loads. The contribution of this paper is that a design methodology is proposed for the inductances and load resistances to realize an equal power distribution. Also, it provides the guideline to adjust the equivalent load resistance and regulate the power distribution, which can be realized by a dc–dc converter at the output side.

II. Working Principle of a Long-Distance Power-Relay System

A. Magnetic Coupler Design

Fig. 1 shows a magnetic field repeater system with a transmitter (L_0) and N power relays ($L_i, i = 1, 2, \ldots, N$).

In this example, the length of the coils is defined as l, the width is defined as w, and the distance between the adjacent coils is defined as d. For simplicity, the coils can be designed in a square shape, which means $l = w$. Therefore, the distance ratio is defined as $r_d = d/l$. Then, the finite-element method is used to simulate the magnetic coupler, in which k_{ij} $(i \neq j)$ represents the coupling coefficient between the ith and jth coils. When the coil distance ratio r_d varies, the couplings between the transmitter coil L_0 and the following power-relay coils are shown in Fig. 2.

Fig. 2 shows that the coupling coefficient between the adjacent coils is much larger than the other couplings. For example, when the coil distance ratio r_d is 1.0, k_{01} is 3.5%, and k_{02} is only 0.05%. Considering the seven times difference, k_{02} can be neglected when r_d is large enough. Therefore, only the adjacent couplings need to be considered in this long-distance system, and they are defined as $k_n = k_{n-1,n}$ $(i = 1, 2, \ldots, N)$.

B. Circuit Working Principle—General Model of Power Distribution

Using the designed magnetic coupler and the simplified coupling model between coils, the circuit topology of the power-relay system is shown in Fig. 3.

In Fig. 3, the resistance R_n $(n = 0, 1, 2, \ldots, N)$ represents the power dissipation of each coil, and the parasitic resistance of the passive component is neglected for simplicity. The angular switching frequency is defined as ω_0, and the capacitor is defined as C_n $(n = 0, 1, 2, \ldots, N)$. Then, the resonant relationship is expressed as

$$\omega_0 = \frac{1}{\sqrt{L_n C_n}}, \quad n = 0, 1, 2, 3, \ldots, N. \tag{1}$$

Also, the mutual inductance between coils is defined as

$$M_n = k_n \sqrt{L_{n-1} L_n}, \quad n = 1, 2, 3, \ldots, N. \tag{2}$$

The magnetic couplings are represented by the current controlled voltage sources, as shown in Fig. 4.

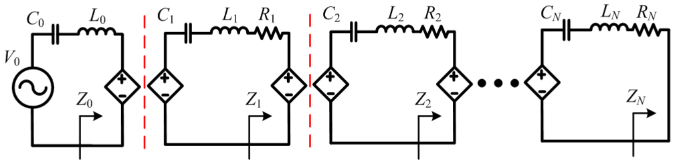

Fig. 4. Equivalent circuit topology of a power-relay system with behavior sources.

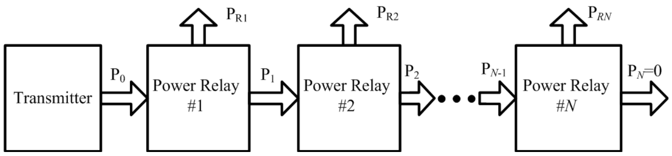

Fig. 5. Power flow and distribution in a power-relay system.

The reflected impedance of the power relay is defined as Z_n ($n = 0, 1, 2, \ldots, N$) and expressed as

$$\begin{cases} Z_N = 0 \\ Z_{n-1} = \dfrac{(\omega_0 M_n)^2}{R_n + Z_n}, \quad n = 1, 2, 3, \ldots, N. \end{cases} \tag{3}$$

In this system, the power transferred by each coil is defined as P_n ($n = 0, 1, 2, \ldots, N$), and the power dissipated by each resistor is defined as P_{Rn} ($n = 1, 2, 3, \ldots, N$). Therefore, the power flow and distribution are shown in Fig. 5.

According to Figs. 4 and 5, the power ratio between the adjacent relays is defined as γ_n ($n = 2, 3, \ldots, N$)

$$\gamma_n = \frac{P_{Rn-1}}{P_{Rn}} = \frac{R_{n-1}}{R_n} \cdot \frac{R_n + Z_n}{Z_{n-1}}, \quad n = 2, 3, \ldots, N. \tag{4}$$

By substituting the definition of Z_n in (3), γ_n is simplified as

$$\begin{cases} \gamma_N = \dfrac{R_{N-1}}{R_N} \cdot \dfrac{R_N^2}{(\omega_0 M_N)^2}\cdot \\ \gamma_n = \dfrac{R_{n-1}}{R_n} \dfrac{\left(1 + \frac{1}{\gamma_{n+1}} + \frac{1}{\gamma_{n+1}\gamma_{n+2}} + \cdots + \frac{1}{\gamma_{n+1}\cdots\gamma_N}\right)^2 R_n^2}{(\omega_0 M_n)^2}, \\ \qquad n = 2, .., (N-1). \end{cases} \tag{5}$$

It shows that the power ratio γ_n is determined by the resistance R_n and the mutual inductances M_n. Therefore, it is meaningful to design R_n and M_n to regulate the power distribution among the power relays. To achieve equal power distribution, there is $\gamma_n = 1$ ($n = 2, 3, \ldots, N$). Then, the parameter relationship is

$$R_{n-1} R_n = \left(\frac{\omega_0 M_n}{N - n + 1}\right)^2, \quad n = 2, 3, \ldots, N. \tag{6}$$

III. Design Examples: Equal Power Distributed System

Section II-B shows the power distribution relates to R_n and M_n. Therefore, this section will present three examples to illustrate the design method to achieve equal power distribution.

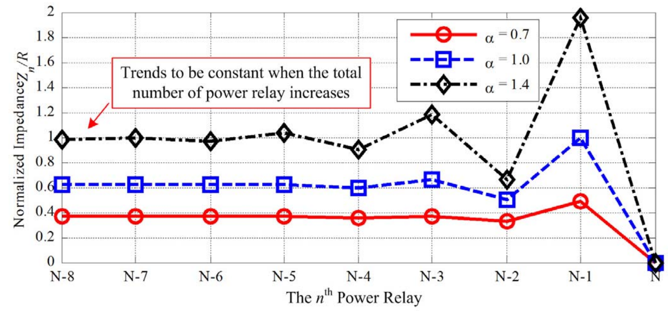

Fig. 6. Normalized impedance Z_n/R ($n = 0, 1, 2, \ldots, N-1$) at different values of α.

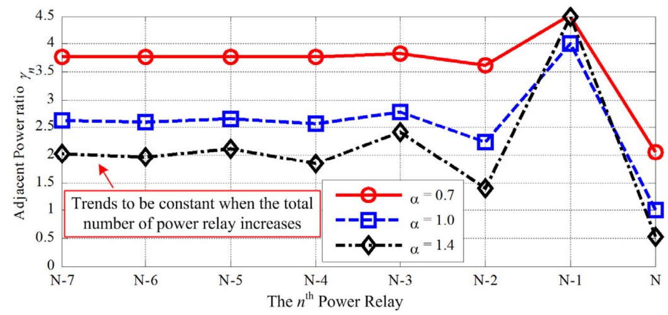

Fig. 7. Power ratio γ_n ($n = 2, 3, \ldots, N$) among power relays at different values of α with identical R_n and M_n.

A. Identical R_n and M_n

In the first example, it is straightforward to have identical coils and load resistances, as shown in the following equation, where α is defined as the ratio of impedance:

$$\begin{cases} M = M_1 = M_2 = \cdots = M_N \\ R = R_1 = R_2 = \cdots = R_N \\ \omega_0 M = \alpha \cdot R. \end{cases} \tag{7}$$

According to (3), the sequence of Z_n ($n = 0, 1, 2, \ldots, N-1$) is calculated as

$$\begin{bmatrix} Z_{N-1} & Z_{N-2} & Z_{N-3} & Z_{N-4} & Z_{N-5} & \cdots \end{bmatrix} = \begin{bmatrix} 1 & \dfrac{1}{\alpha^2+1} & \dfrac{\alpha^2+1}{2\alpha^2+1} & \dfrac{2\alpha^2+1}{3\alpha^2+2} & \dfrac{3\alpha^2+2}{5\alpha^2+3} & \cdots \end{bmatrix} \cdot \alpha^2 \cdot R. \tag{8}$$

It is further summarized in a general form as in (9), as shown at the bottom of the next page. Therefore, for different values of α, the normalized impedance Z_n/R ($n = 0, 1, 2, \ldots, N-1$) is shown in Fig. 6.

It shows that when N is large enough, the impedance Z_0 is approaching a constant value defined as Z. For example, when $\alpha = 1.0$, there is $Z = 0.618\ R$

$$Z = \lim_{N \to \infty} Z_0(N) = \frac{-1 + \sqrt{1 + 4\alpha^2}}{2} \cdot R. \tag{10}$$

Considering the impedance relationship in (8), the power ratio γ_n is calculated as

$$\gamma_n = \frac{P_{Rn-1}}{P_{Rn}} = \frac{1}{\alpha^2} \cdot \left(1 + \frac{Z_n}{R}\right)^2, \quad n = 2, 3, \ldots, N. \tag{11}$$

Then, according to the calculated Z_n/R in Fig. 6, the power ratio γ_n is illustrated in Fig. 7.

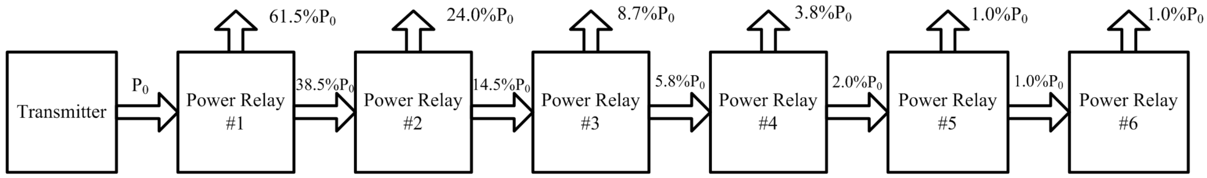

Fig. 8. Example of power flow and distribution when $\alpha = 1.0$ and $N = 6$ with identical R_n and M_n.

Similarly, when N is large enough, the power ratio approaches a constant value. Fig. 7 shows that, in this identical system, the power relay at the near end of the transmitter dissipates more power than the far-end power relay. As a special case, when $\alpha = 1.0$ and $N = 6$, the power distribution is calculated in (12) and shown in Fig. 8

$$[P_{R1} \quad P_{R2} \quad P_{R3} \quad P_{R4} \quad P_{R5} \quad P_{R6}] = [64 \quad 25 \quad 9 \quad 4 \quad 1 \quad 1] \cdot P_{R6}. \quad (12)$$

Fig. 8 shows that, in this identical system, most of the power is dissipated by the first three power relays and it is difficult for the following power relays to acquire sufficient power. When the total number of power relays keeps increasing, the far-end relays cannot receive any power. Therefore, this identical structure is not suitable for the long-distance and multiple-load applications.

B. Identical R_n and Different M_n

In the second example, the load resistances are designed to be identical, but the mutual inductances are different. The parameter relationship is expressed as

$$R = R_1 = R_2 = \cdots = R_N. \quad (13)$$

According to (6), to realize equal power distribution, the mutual inductance M_n $(n = 2, 3, \ldots, N)$ should satisfy

$$\omega_0 M_n = (N - n + 1) \cdot R, \quad n = 2, 3, 4, \ldots, N. \quad (14)$$

Since there is $k = k_1 = k_2 = \cdots = k_N$, the self-inductance L_n $(n = 1, 2, \ldots, N)$ of each coil is calculated as follows.

When $(N - n)$ is an even number, such as $2, 4, 6, \ldots$, the self-inductance is expressed as

$$\sqrt{L_n} = \frac{2}{1} \cdot \frac{4}{3} \cdot \frac{6}{5} \cdot \cdots \cdot \frac{N-n}{N-n-1} \cdot \sqrt{L_N}. \quad (15)$$

When $(N - n)$ is an odd number, such as $3, 5, 7, \ldots$, the self-inductance is expressed as

$$\sqrt{L_n} = \frac{3}{2} \cdot \frac{5}{4} \cdot \frac{7}{6} \cdot \cdots \cdot \frac{N-n}{N-n-1} \cdot \sqrt{L_{N-1}}. \quad (16)$$

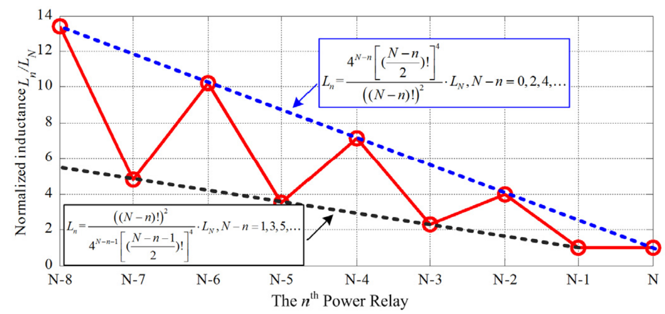

Fig. 9. Normalized inductance L_n/L_N of different power relays with identical R_n and different M_n.

To simplify the coil design, it is assumed $L_{N-1} = L_N$. There is $R = k\omega_0 L_N$, and L_n $(n = 1, 2, \ldots, N)$ is summarized as

$$L_n = \begin{cases} \dfrac{4^{N-n}\left[(\frac{N-n}{2})!\right]^4}{((N-n)!)^2} \cdot L_N, & N - n = 0, 2, 4, \ldots \\ \dfrac{((N-n)!)^2}{4^{N-n-1}\left[(\frac{N-n-1}{2})!\right]^4} \cdot L_N, & N - n = 1, 3, 5, \ldots. \end{cases} \quad (17)$$

Therefore, the normalized inductance L_n/L_N $(n = 1, 2, \ldots, N)$ is illustrated in Fig. 9.

Fig. 9 shows that when the number of power relays increases, the self-inductances of the near-end power relays tend to be much larger than those of the far-end ones. For example, when the number is 9, the largest self-inductance $L_1 = 13.4L_9$. Considering the inductance is proportional to the square of the turn number, L_1 needs to have 3.7 times of turns compared to L_9, which is difficult to realize in the practical implementation.

C. Identical M_n and Different R_n

In the third example, the coils are designed to be identical for easy implementation, and the load resistances are different, resulting in the parameter relationship as follows, where α is also defined as the impedance ratio:

$$\begin{cases} M = M_1 = M_2 = M_3 = \cdots = M_N \\ \omega_0 M_N = \alpha \cdot R_N. \end{cases} \quad (18)$$

$$Z_n = \frac{\alpha^2 \cdot \left(\frac{1+\sqrt{1+4\alpha^2}}{2\sqrt{1+4\alpha^2}} \cdot \left(\frac{1+\sqrt{1+4\alpha^2}}{2}\right)^{N-1-n} + \frac{-1+\sqrt{1+4\alpha^2}}{2\sqrt{1+4\alpha^2}} \cdot \left(\frac{1-\sqrt{1+4\alpha^2}}{2}\right)^{N-1-n} \right) \cdot R}{\frac{1+\sqrt{1+4\alpha^2}+2\alpha^2}{2\sqrt{1+4\alpha^2}} \cdot \left(\frac{1+\sqrt{1+4\alpha^2}}{2}\right)^{N-1-n} + \frac{-1+\sqrt{1+4\alpha^2}-2\alpha^2}{2\sqrt{1+4\alpha^2}} \cdot \left(\frac{1-\sqrt{1+4\alpha^2}}{2}\right)^{N-1-n}}, \quad n = 0, \ldots, N-1 \quad (9)$$

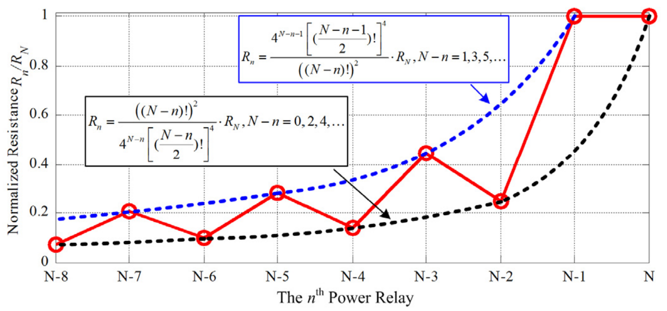

Fig. 10. Normalized resistance R_n/R_N of different power relays with identical M_n and different R_n.

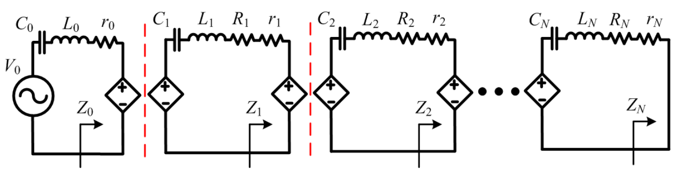

Fig. 11. Equivalent circuit topology of a power-relay system considering the parasitic resistances of passive components.

According to (6), to achieve equal power distribution, there is $R_{N-1} = \alpha^2 R_N$, and the other R_n should satisfy the following relations.

When $(N-n)$ is an even number $(2, 4, \ldots)$

$$R_n = \left(\frac{1}{2}\cdot\frac{3}{4}\cdot\frac{5}{6}\cdot\cdots\cdot\frac{N-n-1}{N-n}\right)^2 \cdot R_N. \tag{19}$$

When $(N-n)$ is an odd number $(3, 5, \ldots)$

$$R_n = \left(\frac{2}{3}\cdot\frac{4}{5}\cdot\frac{6}{7}\cdot\cdots\cdot\frac{N-n-1}{N-n}\right)^2 \cdot \alpha^2 \cdot R_N. \tag{20}$$

Therefore, when $\alpha = 1.0$, the normalized resistance R_n/R_N is summarized and shown in Fig. 10.

Fig. 10 shows that, in order to achieve equal power distribution, the load resistance tends to decrease with the increasing number of power relays. For example, when $N = 9$, there is $R_1 = 0.075R_9$. Therefore, it requires regulating the impedance of the load resistance to adjust the power distribution. In a practical application, it can be achieved by connecting a controllable dc–dc converter to each stage.

IV. Discussion: Power Transfer Capability of a Multiple-Relay System

A. Impact of Parasitic Resistances

Considering the parasitic resistances of the passive components, the circuit topology is shown in Fig. 11.

The quality factor of the passive components is defined as Q, and the parasitic resistance is defined as r_n

$$r_n = \omega_0 L_n/Q, \quad n = 0, 1, 2, 3, \ldots, N. \tag{21}$$

The reflected impedance is expressed as

$$\begin{cases} Z_N = 0 \\ Z_{n-1} = \dfrac{(\omega_0 M_n)^2}{R_n + r_n + Z_n}, \quad n = 1, 2, 3, \ldots, N. \end{cases} \tag{22}$$

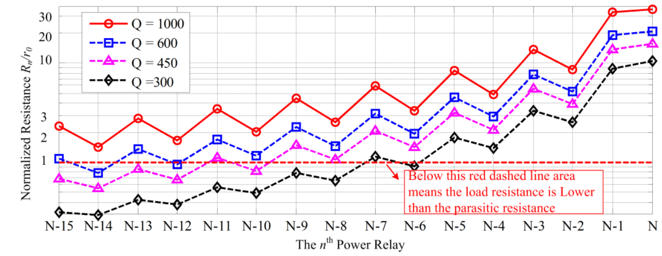

Fig. 12. Normalized resistance R_n/r_0 of different power relays with identical M_n and different R_n at different quality factor Q.

Then, according to (22), the power ratio between the adjacent power relays is expressed as in (23), as shown at the bottom of the next page.

To achieve equal power distribution, there is $\gamma_n = 1$ $(n = 2, 3, \ldots, N)$, and the parameter relationship is in the following equation:

$$\begin{cases} R_{N-1} = R_N \cdot \dfrac{(\omega_0 M_N)^2}{(R_N + r_N)^2} \\ R_{n-1} = R_n \dfrac{(\omega_0 M_n)^2}{\left[(N-n)R_n + r_n + \left(\frac{r_{n+1}}{R_{n+1}} + \cdots + \frac{r_N}{R_N}\right)R_n\right]^2}, \\ \qquad n = 2, 3, .., (N-1). \end{cases} \tag{24}$$

In an identical M_n and different R_n examples, the parasitic resistance is represented by $r_0 = r_1 = r_2 = \ldots = r_N$. Fig. 10 indicates that the load resistance decreases with the increasing number of power relays. There is a risk that the load resistance is smaller than the parasitic resistances, which affects the effectiveness of the power transfer process. Therefore, according to (24), the normalized resistance R_n/r_0 is calculated and shown in Fig. 12.

Fig. 12 shows that the parasitic resistance tends to reduce the load resistance. The lower is the quality factor, the lower the load resistance is. The load resistance is also compared to the parasitic resistance as the red dashed line. The area below the red dashed line means that the load resistance is lower than the parasitic resistance, which should be avoided. Therefore, Fig. 12 provides the power transfer capability of a multiple-relay system and the guideline to design the parameters of a real application. For example, when $Q = 450$, Fig. 12 shows that the load resistance is lower than the parasitic resistance as long as the total number of the power relay reaches 11, which means the recommended maximum number of the power relays is 11.

B. Efficiency Analysis

According to Fig. 11, when the parasitic resistances are considered, the system transfer efficiency is affected. The transfer efficiency of each power relay is defined as η_n $(n = 1, 2, \ldots, N)$, and the total efficiency is defined as η_0. Then, the efficiency is calculated and expressed as in (25).

Considering (21)–(24), the total power transfer efficiency η_0 is calculated and shown in Fig. 13. It shows that the efficiency increases with the increasing quality factor Q, which

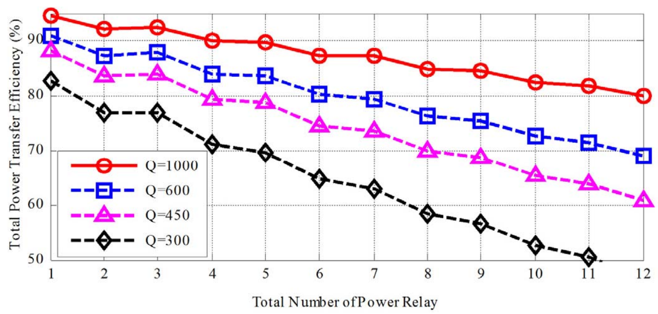

Fig. 13. Total transfer efficiency η_0 with identical M_n and different R_n at different quality factor Q and different number of power relays.

is very straightforward and consistent with a traditional two-coil system. Meanwhile, when the total number of power relays increases, there is more power loss dissipated in the system, resulting in lower transfer efficiency

$$\begin{cases} \eta_N = \dfrac{R_N}{R_N + r_N} \\ \eta_n = \dfrac{R_n}{R_n + r_n + Z_n} + \dfrac{Z_n}{R_n + r_n + Z_n} \cdot \eta_{n+1}, \\ \qquad n = 1, 2, 3, \ldots, (N-1) \\ \eta_0 = \dfrac{Z_0}{Z_0 + r_0} \cdot \eta_1. \end{cases} \tag{25}$$

Fig. 13 shows also an important guideline to design a power-relay system. For the given quality factor and transfer efficiency, it can provide the maximum allowable number of power relays, which relates to the power transfer capability and total transfer distance. For example, when $Q = 450$ and the total number of power relays is 8, the system efficiency can reach 70%.

V. System Implementation and Experiments

A. Circuit Parameter Design

According to the previous analysis, the identical M_n and different R_n examples are selected to realize an equal power distributed system. Then, according to Fig. 11 and (25), the system power is calculated as

$$P_{\text{out}} = \frac{|V_0|^2}{(Z_0 + r_0)^2} \cdot \eta_0. \tag{26}$$

Using (24)–(26), the circuit parameters of an equal power distributed system with eight power relays are calculated and designed. The detailed design process is shown in Fig. 14.

In the design process, the target is to satisfy the power and efficiency requirement, and (24)–(26) and Figs. 12 and 13 are used as the guidelines to assist the calculation. The designed values of the circuit components are summarized in Table I.

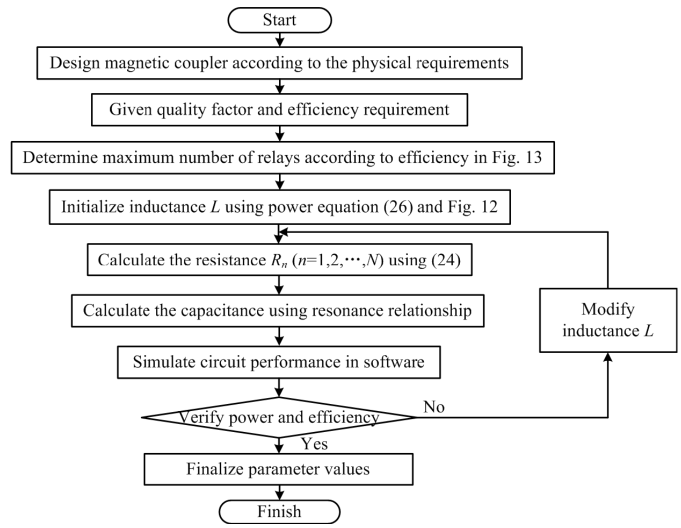

Fig. 14. Design process of an equal power distributed IPT system.

TABLE I

Specifications and Circuit Parameters of an Equal Power Distributed System With Eight Power Relays

Parameter	Design Value	Parameter	Design Value
V_{in}	140 V	l (w)	400 mm
f_{sw}	1 MHz	d	400 mm
L_0~L_8	110 µH	k	0.035
C_0~C_8	230.3 pF	N	8
r_0~r_8	1.5 Ω	Q	450
R_1	3.22 Ω	R_2	2.23 Ω
R_3	4.86 Ω	R_4	3.30 Ω
R_5	8.48 Ω	R_6	6.00 Ω
R_7	21.39 Ω	R_8	24.19 Ω

In this design, the switching frequency is 1 MHz. The transmitter inductance L_0 can be slightly tuned to regulate the system power without affecting the property of equal power distribution. For example, when L_0 is tuned to 99 μH, each power relay can dissipate about 90-W power. The resistances R_1 and R_2 are much smaller than R_8, which is consistent with Fig. 10. With the increasing number of power relays, the load resistance decreases, and it could be even smaller than r_0, which limits the transfer capability of a multiple-relay system.

B. Experimental Prototype Design

Using the parameters in Table I, a prototype of the power-relay system is implemented in Fig. 15. There are one

$$\begin{cases} \gamma_N = \dfrac{R_{N-1}}{R_N} \cdot \dfrac{(R_N + r_N)^2}{(\omega_0 M_N)^2} \\ \gamma_n = \dfrac{R_{n-1}}{R_n} \cdot \dfrac{\left[\left(1 + \frac{1}{\gamma_{n+1}} + \cdots + \frac{1}{\gamma_{n+1}\cdots\gamma_N}\right) R_n + r_n + \left(\frac{r_{n+1}}{R_{n+1}} \cdot \frac{1}{\gamma_{n+1}} + \cdots + \frac{r_N}{R_N} \cdot \frac{1}{\gamma_{n+1}\cdots\gamma_N}\right) R_n\right]^2}{(\omega_0 M_n)^2}, \quad n = 2, 3, \ldots, (N-1) \end{cases} \tag{23}$$

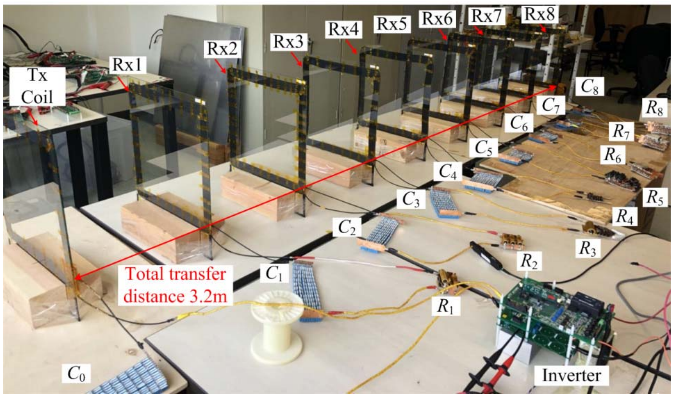

Fig. 15. Experimental setup of a power-relay system with eight resistive loads and 3.2-m transfer distance.

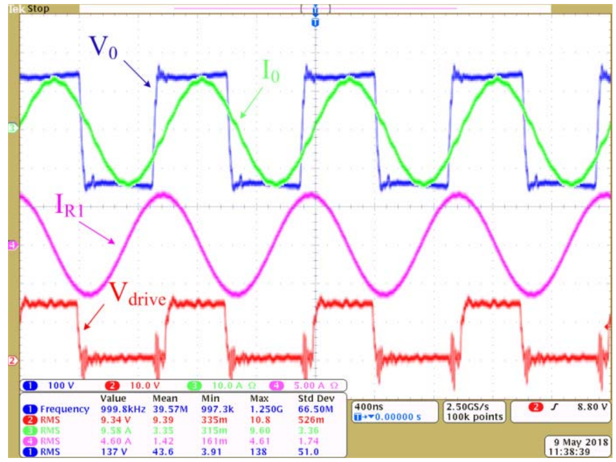

Fig. 16. Experimental waveforms of the voltages and currents. Ch1 (blue): V_0 input voltage. Ch2 (red): V_{drive} driver voltage. Ch3 (green): I_0 input current. Ch4 (pink): I_{R1} current of the first power relay.

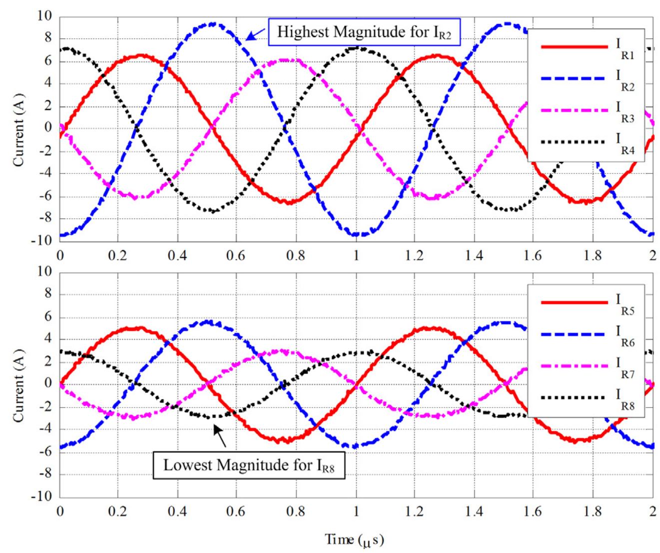

Fig. 17. Experimental waveforms of the currents in the eight power relays.

transmitter and eight relay coils. The coils are identical and wound by 2175-strand AWG40 Litz-wire to reduce the skin effect. They are installed on a glass and wood fixture, and no ferrite is used. The coil has 11 turns, and its size is 400 mm $\times$ 400 mm. In the high-frequency range, the influence of the interturn parasitic capacitance to the coil needs to be considered. Then, the network analyzer is used to measure the high-frequency property of the coil, which shows that the self-resonant frequency is much higher than 1 MHz. The adjacent coil distance is 400 mm, resulting in a total transfer distance of 3.2 m. An inverter with silicon carbide devices (C2M0080120D) can provide a switching frequency of 1 MHz.

Compensation capacitors are connected with the coils to establish resonances. Measurement shows that the quality factor of a single coil is 1100, and the quality factor of the resonant loop is about 450, which reaches the designed value in Table I. For each power relay, a resistor is connected as the load to dissipate power. Multiple resistors are connected in series and parallel to achieve the resistance values in Table I.

C. Experimental Results

In the experiment, the compensation capacitances are tuned to achieve perfect resonances with the inductors. The resistances are tuned to achieve equal power distribution among the power relays. Measurements show that the experimental load resistances closely agree with the calculation values in Table I. In the experiments, the transmitter inductance L_0 is slightly tuned to regulate the power. With the input voltage of 140 V, the experimental waveforms are shown in Fig. 16.

Fig. 16 shows that the input voltage V_0 is almost in phase with the input current I_0, which means the reactive power in the circuit is limited to maintain relatively high efficiency. The slight phase difference between V_0 and I_0 can help achieve soft switching for the MOSFETs, and the switching loss is, therefore, reduced. The driver signal V_{drive} shows that the noise is lower than the threshold voltage of the MOSFETs, and it is safe to use this signal to drive the devices. The circulating current I_{R1} in the first power relay is also measured. It is about 90° out of phase with the input current I_0 and can be used to calculate the power dissipation of the load.

The experimental waveforms of the currents in the eight power relays are shown and compared in Fig. 17.

The circulating current in each power relay is measured by an oscilloscope, and the data of waveforms are extracted and redrawn by MATLAB. Experiments show that the currents in the adjacent coils are 90° out of phase, which validates that the capacitors have fully compensated the self-inductances of the coils. In this design, since the load resistance R_2 is the smallest, the highest current occurs in the second power relay. Also, since R_8 is the largest, the lowest current occurs in the last power relay. In the experiments, considering the high circulating currents in the coils, it is important to maintain the insulation of the coil to avoid any concern of arcing.

Using the current magnitudes in Fig. 17 and the measured resistances, the output power of the power relays is shown in Fig. 18. Meanwhile, according to the measured parasitic resistances of the passive components, the power loss in the transmitter and power relays is also provided.

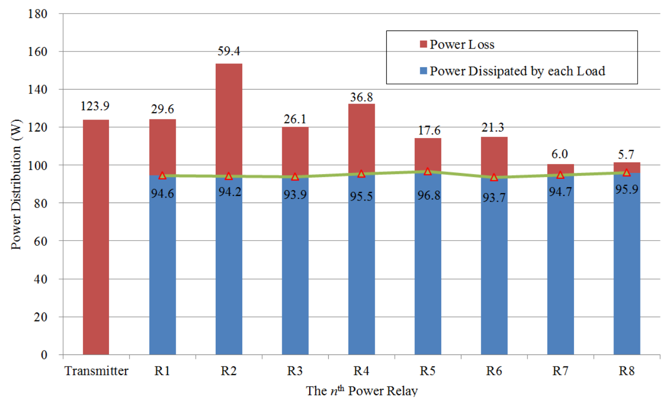

Fig. 18. Experimental results of the dissipated power and power loss in the transmitter and the eight power relays.

Fig. 18 shows that equal power distribution among the eight power relays is achieved. The maximum dissipated power is 96.8 W, and the minimum dissipated power is 93.7 W, resulting in a power variation within ±2.0%. The total dissipated power by the eight load resistances is 759.3 W. The power loss analysis shows that the transmitter dissipates the most loss (123.9 W) because the circulating current in the transmitter is the highest. In the eight power relays, the second relay dissipates 59.4-W loss. It needs to be pointed out that the power loss occurs in both the coils and capacitors. Therefore, in the prototype, multiple capacitors are connected in series and parallel to avoid too high-temperature rise. The total power loss is about 326.4 W, resulting in a power transfer efficiency of 70%, which validates the efficiency analysis in Fig. 13.

VI. Conclusion

This paper aims to provide the design methodology of a distributed power-relay system from two aspects. First, we modeled the power distribution of a power-relay system with multiple loads, showing the inductances and resistances determine the power distribution. It also provided the guideline to design a distributed system with equal power load at each stage. Second, we studied the power transfer capability of the power-relay system and derived the maximum number of power relays and the maximum achievable efficiency with given quality factor and efficiency requirement. The identical M_n and different R_n examples are designed and implemented to validate the proposed power-relay system. The experimental results demonstrate that this system can achieve relatively high efficiency over a long distance. For example, using eight 400 mm × 400 mm coils, 759.3-W power can be transferred along 3.2 m with efficiency of 70.0%. The accomplishment of this paper can be applied to the long-distance and multiple-load applications, ensuring that each load can receive enough power efficiently in a distributed system.

References

[1] G. A. Covic and J. T. Boys, "Inductive power transfer," *Proc. IEEE*, vol. 101, no. 6, pp. 1276–1289, Jun. 2013.
[2] Z. Huang, S.-C. Wong, and C. K. Tse, "Control design for optimizing efficiency in inductive power transfer systems," *IEEE Trans. Power Electron.*, vol. 33, no. 5, pp. 4523–4534, May 2018.
[3] C. T. Rim and C. Mi, *Wireless Power Transfer for Electric Vehicles and Mobile Devices*. Hoboken, NJ, USA: Wiley, 2017.
[4] S. Y. R. Hui, W. X. Zhong, and C. K. Lee, "A critical review of recent progress in mid-range wireless power transfer," *IEEE Trans. Power Electron.*, vol. 29, no. 9, pp. 4500–4511, Sep. 2014.
[5] S. Y. R. Hui, "Past, present and future trends of non-radiative wireless power transfer," *CPSS Trans. Power Electron. Appl.*, vol. 1, no. 1, pp. 83–91, Dec. 2016.
[6] E. S. Lee, J. S. Choi, H. S. Son, S. H. Han, and C. T. Rim, "Six degrees of freedom wide-range ubiquitous IPT for IoT by DQ magnetic field," *IEEE Trans. Power Electron.*, vol. 32, no. 11, pp. 8258–8276, Nov. 2017.
[7] E. S. Lee, B. G. Choi, J. S. Choi, D. T. Nguyen, and C. T. Rim, "Wide-range adaptive IPT using dipole-coils with a reflector by variable switched capacitance," *IEEE Trans. Power Electron.*, vol. 32, no. 10, pp. 8054–8070, Oct. 2017.
[8] B. H. Choi, V. X. Thai, E. S. Lee, J. H. Kim, and C. T. Rim, "Dipole-coil-based wide-range inductive power transfer systems for wireless sensors," *IEEE Trans. Ind. Electron.*, vol. 63, no. 5, pp. 3158–3167, May 2016.
[9] W. X. Zhong, C. K. Lee, and S. Y. R. Hui, "General analysis on the use of Tesla's resonators in domino forms for wireless power transfer," *IEEE Trans. Ind. Electron.*, vol. 60, no. 1, pp. 261–270, Jan. 2013.
[10] R. Hua, G. Kalra, V. Wang, and A. P. Hu, "Extending the inductive power transfer range by using passive power repeaters," in *Proc. 12th IEEE Conf. Ind. Electron. Appl. (ICIEA)*, Jun. 2017, pp. 1718–1722.
[11] B. Luo, S. Wu, and N. Zhou, "Flexible design method for multi-repeater wireless power transfer system based on coupled resonator bandpass filter model," *IEEE Trans. Circuits Syst. I, Reg. Papers*, vol. 61, no. 11, pp. 3288–3297, Nov. 2014.
[12] X. Dai, L. Li, X. Yu, Y. Li, and Y. Sun, "A novel multi-degree freedom power pickup mechanism for inductively coupled power transfer system," *IEEE Trans. Magn.*, vol. 53, no. 5, May 2017, Art. no. 8600107.
[13] X. Liu and G. Wang, "A novel wireless power transfer system with double intermediate resonant coils," *IEEE Trans. Ind. Informat.*, vol. 63, no. 4, pp. 2174–2180, Apr. 2016.
[14] K. Lee and S. H. Chae, "Power transfer efficiency analysis of intermediate-resonator for wireless power transfer," *IEEE Trans. Power Electron.*, vol. 33, no. 3, pp. 2484–2493, Mar. 2018.
[15] Y. Li, K. Song, C. Zhu, G. Wei, and R. Lu, "Efficiency optimizing and load matching analysis for the weak-coupling wireless power transfer system using a repeating coil," in *Proc. IEEE PELS Workshop Emerg. Technol., Wireless Power Transf. (WoW)*, Oct. 2016, pp. 31–34.
[16] M. Fu, H. Yin, M. Liu, Y. Wang, and C. Ma, "A 6.78 MHz multiple-receiver wireless power transfer system with constant output voltage and optimum efficiency," *IEEE Trans. Power Electron.*, vol. 33, no. 6, pp. 5330–5340, Jun. 2018.
[17] M. Fu, T. Zhang, C. Ma, and X. Zhu, "Efficiency and optimal loads analysis for multiple-receiver wireless power transfer systems," *IEEE Trans. Microw. Theory Techn.*, vol. 63, no. 3, pp. 801–812, Mar. 2015.
[18] W. X. Zhong, C. K. Lee, and S. Y. Hui, "Wireless power domino-resonator systems with noncoaxial axes and circular structures," *IEEE Trans. Power Electron.*, vol. 27, no. 11, pp. 4750–4762, Nov. 2012.
[19] M. Q. Nguyen, Y. Chou, D. Plesa, S. Rao, and J.-C. Chiao, "Multiple-inputs and multiple-outputs wireless power combining and delivering systems," *IEEE Trans. Power Electron.*, vol. 30, no. 11, pp. 6254–6263, Nov. 2015.
[20] D. Ahn and S. Hong, "Effect of coupling between multiple transmitters or multiple receivers on wireless power transfer," *IEEE Trans. Ind. Electron.*, vol. 60, no. 7, pp. 2602–2613, Jul. 2013.
[21] Y. Zhang, T. Lu, Z. Zhao, F. He, K. Chen, and L. Yuan, "Selective wireless power transfer to multiple loads using receivers of different resonant frequencies," *IEEE Trans. Power Electron.*, vol. 30, no. 11, pp. 6001–6005, Nov. 2015.
[22] Y. Zhang, T. Lu, Z. Zhao, K. Chen, F. He, and L. Yuan, "Wireless power transfer to multiple loads over various distances using relay resonators," *IEEE Microw. Wireless Compon. Lett.*, vol. 25, no. 5, pp. 337–339, May 2015.
[23] C. Zhang, W. Zhong, X. Liu, and S. Y. R. Hui, "A fast method for generating time-varying magnetic field patterns of mid-range wireless power transfer systems," *IEEE Trans. Power Electron.*, vol. 30, no. 3, pp. 1513–1520, Mar. 2015.
[24] S. A. Mirbozorgi, H. Bahrami, M. Sawan, and B. Gosselin, "A smart cage with uniform wireless power distribution in 3D for enabling long-term experiments with freely moving animals," *IEEE Trans. Biomed. Circuits Syst.*, vol. 10, no. 2, pp. 424–434, Apr. 2016.

[25] Q. Zhu, M. Su, Y. Sun, W. Tang, and A. P. Hu, "Field orientation based on current amplitude and phase angle control for wireless power transfer," *IEEE Trans. Ind. Electron.*, vol. 65, no. 6, pp. 4758–4770, Jun. 2018.

[26] J. Kim, H.-C. Son, D.-H. Kim, and Y.-J. Park, "Optimal design of a wireless power transfer system with multiple self-resonators for an LED TV," *IEEE Trans. Consum. Electron.*, vol. 58, no. 3, pp. 775–780, Aug. 2012.

[27] M. Q. Nguyen, S. Dubey, S. Rao, and C. Chiao, "Wireless power transfer via air and building materials using multiple repeaters," in *Proc. Texas Symp. Wireless Microw. Circuits Syst.*, Apr. 2014, pp. 1–4.

[28] Z. Zhang, K. T. Chau, C. Qiu, and C. Liu, "Energy encryption for wireless power transfer," *IEEE Trans. Power Electron.*, vol. 30, no. 9, pp. 5237–5246, Sep. 2015.

[29] C. Zhang, D. Lin, N. Tang, and S. Y. R. Hui, "A novel electric insulation string structure with high-voltage insulation and wireless power transfer capabilities," *IEEE Trans. Power Electron.*, vol. 33, no. 1, pp. 87–96, Jan. 2018.

Fei Lu (S'12–M'17) received the B.S. and M.S. degrees in electrical engineering from the Harbin Institute of Technology, Harbin, China, in 2010 and 2012, respectively, and the Ph.D. degree in electrical engineering from the University of Michigan, Ann Arbor, MI, USA, in 2017.

He is currently an Assistant Professor with the Department of Electrical and Computer Engineering, Drexel University, Philadelphia, PA, USA. His current research interests include power electronics and the application of electric vehicle charging.

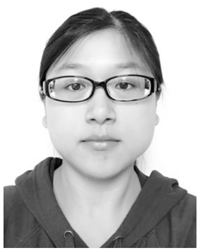

Hua Zhang (S'14–M'17) received the B.S., M.S., and Ph.D. degrees in electrical engineering from Northwestern Polytechnical University, Xi'an, China, in 2011, 2014, and 2017, respectively, and the joint Ph.D. degree from the University of Michigan-Dearborn, Dearborn, MI, USA, in 2015.

In 2015, she joined San Diego State University, San Diego, CA, USA. She is currently a Post-Doctoral Research Associate with Drexel University, Philadelphia, PA, USA. Her current research interests include charging of electric vehicles.

Weiguo Li (M'01) received the B.S. degree in electrical engineering from Northeast Dianli University, Jilin, China, in 1996, the M.S. degree in electrical engineering from the China Electric Power Research Institute, Beijing, China, in 2006, and the Ph.D. degree in electrical engineering from North China Electric Power University, Beijing, in 2013.

He is currently with the State Key Laboratory of Advanced Power Transmission Technology, Global Energy Interconnection Research Institute, Beijing. His current research interests include flexible ac transmission systems and power systems.

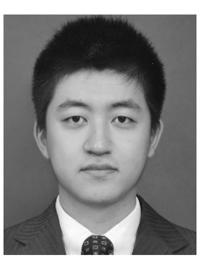

Zhe Zhou received the B.E. degree in measure and control technology and instrumentations from the Changchun University of Science and Technology, Changchun, China, in 2011, and the M.S. degree in power electronics and power drives from Tianjin University, Tianjin, China, in 2014.

He is currently with the State Key Laboratory of Advanced Power Transmission Technology, Global Energy Interconnection Research Institute, Beijing, China. His current research interests include solid-state transformers.

Chong Zhu (M'17) received the B.S. degree in electrical engineering from the China University of Mining and Technology, Xuzhou, China, in 2010, and the Ph.D. degree in electrical engineering from Zhejiang University, Hangzhou, China, in 2016.

He is currently a Post-Doctoral Researcher with San Diego State University, San Diego, CA, USA. His current research interests include battery thermal management and ac/dc power conversion.

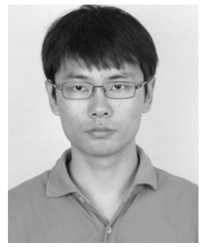

Chenwen Cheng received the B.S. and Ph.D. degrees in electrical engineering from Zhejiang University, Hangzhou, China, in 2012 and 2017, respectively.

He is currently a Post-Doctoral Researcher with San Diego State University, San Diego, CA, USA. His current research interests include motor control, renewable power generation, and wireless power transfer technologies.

Zhanfeng Deng received the B.S. and M.S. degrees in welding technology and equipment from Jilin Polytechnical University, Changchun, China, in 1996, and the Ph.D. degree in electrical engineering from Tsinghua University, Beijing, China, in 2003.

He is currently with the State Key Laboratory of Advanced Power Transmission Technology, Global Energy Interconnection Research Institute, Beijing. His current research interests include flexible ac transmission systems and power systems.

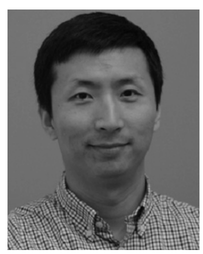

Xi Chen (S'07–M'13–SM'16) received the B.Eng. degree in information engineering from Beijing Technology and Business University, Beijing, China, in 2003, the M.Sc. degree in digital signal processing from the Kings College London, University of London, London, U.K., in 2005, and the Ph.D. degree in electronic and information engineering from The Hong Kong Polytechnic University, Hong Kong, in 2009.

In 2014, he joined the Global Energy Interconnection Research Institute North America, San Jose, CA, USA, where he is currently a Chief Information Officer. His current research interests include Internet of Things, smart grid, electric vehicle charging infrastructure, and complex networks analysis and its applications.

Chunting Chris Mi (S'00–A'01–M'01–SM'03–F'13) received the B.S.E.E. and M.S.E.E. degrees in electrical engineering from Northwestern Polytechnical University, Xi'an, China, in 1985 and 1988, respectively, and the Ph.D. degree in electrical engineering from the University of Toronto, Toronto, ON, Canada, in 2001.

From 2001 to 2015, he was with the University of Michigan-Dearborn, Dearborn, MI, USA. He is currently a Professor and the Chair of electrical and computer engineering and the Director of the Department of Energy—funded Graduate Automotive Technology Education Center for Electric Drive Transportation, San Diego State University, San Diego, CA, USA.